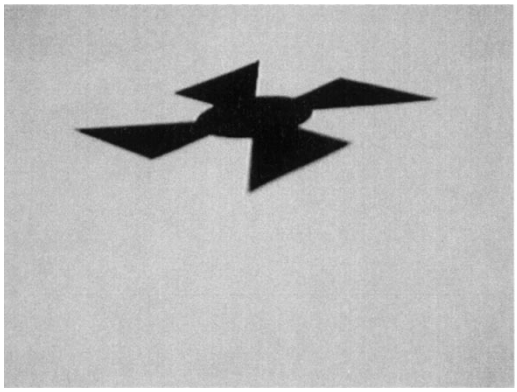

(a)

(b)

Fig. 5. (a) Real image of a rotationally symmetric shape. (b) Recovered pattern by using the proposed method.

demonstrate the robustness of this method to noise and digitization errors.

The output images of the last experiment are imperfect RSS. This is due to the nonlinear distortion caused by the camera lens. In such situation, orthographic projection assumption is no longer valid. However, fairly well results are provided and this indicates the usability of our method to imperfect rotational symmetry. To achieve better results , a camera calibration procedure may be placed before our system. It is beyond the scope of this research.

V. Conclusion

In this work, we propose an $\mathcal{O}(n)$ algorithm to recover the skewed RSS. Our algorithm needs no numeric method and no information about the number of folds. Since this method is based on the moments, it does not rely on smooth or continuous contours and is robust to noise or digitization errors but assumes there is no occlusion. We do not intend to finding the axis of symmetry, because a given RSS may not have any axis of reflective symmetry. However, it does have axes, several kinds of axes are proposed by previous researchers [1]–[4].

The experimental results confirm our derivations of constraints and show availability of our algorithm. Shapes with and without reflective symmetry are all presented. The algorithm gives accurate estimation of the skew parameters α and β.

After applying our algorithm, any of the algorithms proposed in [1]–[5] can be used to find the axes and normalize the deskewed RSS. Thus, the whole normalization procedure is completed.

References

[1] W.-H. Tsai and S.-L. Chou, "Detection of generalized principal axes in rotationally symmetric shapes," *Pattern Recognit.*, vol. 24, pp. 95–104, 1991.

[2] S.-C. Pei and C.-N. Lin, "Normalization of rotationally symmetric shapes for pattern recognition," *Pattern Recognit.*, vol. 25, pp. 913–920, 1992.

[3] J.-C. Lin, "Universal principal axes: An easy-to-construct tool useful in defining shape orientations for almost every kind of shape," *Pattern Recognit.*, vol. 26, pp. 485–493, 1993.

[4] J.-C. Lin, W.-H. Tsai, and J.-A. Chen, "Detecting number of folds by a simple mathematical property," *Pattern Recognit. Lett.*, vol. 15, pp. 1081–1088, 1994.

[5] R. K. K. Yip, W. C. Y. Lam, P. K. S. Tam, and D. N. K. Leung, "A Hough transform technique for the detection of rotational symmetry," *Pattern Recognit. Lett.*, vol. 15, pp. 919–928, 1994.

[6] T. Kanade, "Recovery of the three-dimensional shape of an object from a single view," *Artif. Intell.* vol. 17, pp. 409–460, 1981.

[7] S. A. Friedberg, "Finding axes of skewed symmetry," *Comput. Vis., Graph., Image Process.*, vol. 34, pp. 138–155, 1986.

[8] A. D. Gross and T. E. Boult, "Analyzing skewed symmetries," *Int. J. Comput. Vis.*, vol. 13, pp. 91–111, 1994.

[9] M.-K. Hu, "Visual pattern recognition by moment invariants," *IRE Trans. Inform. Theory*, vol. IT-8, pp. 179–187, 1962.

Tri-State Median Filter for Image Denoising

Tao Chen, Kai-Kuang Ma, and Li-Hui Chen

***Abstract*—In this work, a novel nonlinear filter, called *tri-state median* (TSM) filter, is proposed for preserving image details while effectively suppressing impulse noise. We incorporate the standard median (SM) filter and the *center weighted median* (CWM) filter into a noise detection framework to determine whether a pixel is corrupted, before applying filtering unconditionally. Extensive simulation results demonstrate that the proposed filter consistently outperforms other median filters by balancing the tradeoff between noise reduction and detail preservation.**

***Index Terms*—Impulse noise, median filter, noise detection.**

I. Introduction

Digital images are often corrupted by *impulse noise* during the acquisition or transmission through communication channels. Consequently, some pixel intensities are inevitably altered while others remain noise-free. The image model containing impulse noise with probability of occurrence p can be described as follows:

$$X_{ij} = \begin{cases} N_{ij}, & \text{with probability } p; \\ S_{ij}, & \text{with probability } 1-p \end{cases} \tag{1}$$

where S_{ij} denotes the noiseless image pixel and N_{ij} the noise substituting for the original pixel.

In order to remove impulse noise and enhance image quality, the median filter has been extensively studied and presented in the literature (e.g., [1] and [2]). Median filtering being a nonlinear filtering technique, it is generally superior to linear filtering (e.g.,

Manuscript received June 30, 1998; revised April 27, 1999. The associate editor coordinating the review of this manuscript and approving it for publication was Dr. Henri Maitre.

T. Chen is with the School of Computer Science and Software Engineering, Monash University, Clayton Campus, Vic. 3168, Australia (e-mail: tchen@cs.monash.edu.au).

K.-K. Ma and L.-H. Chen are with the School of Electrical and Electronic Engineering, Nanyang Technological University, Singapore, Republic of Singapore, 639798 (e-mail: elhchen@ntu.edu.sg).

Publisher Item Identifier S 1057-7149(99)09349-5.

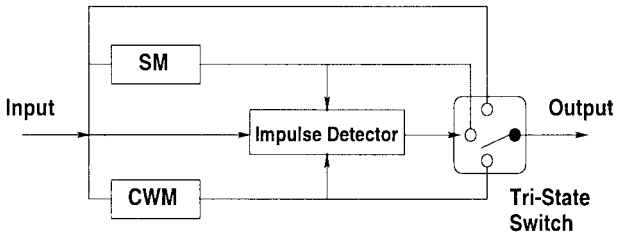

Fig. 1. Block diagram of proposed tri-state median filtering scheme. Note that the straight line is equivalent to the *identity* filter.

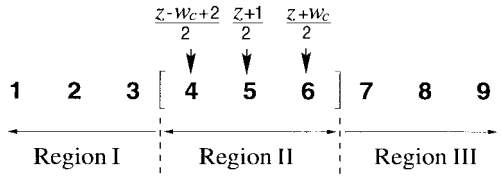

Fig. 2. An illustration of sorted sequence and its three partitioned regions in the case of $z = 9$ and $w_c = 3$. The new median (i.e., the output of CWM filter) is different (unless numerical coincidence) according to which region the origin pixel value X_c is fallen in.

moving average filter) on effectively suppressing impulse noise. Unfortunately, it tends to blur fine details or destroy edges while filtering out impulses.

To trade off detail preservation against noise reduction, Ko and Lee [3] proposed the *center weighted median* (CWM) filters, in which they applied a weight adjustment to the center or origin pixel within the sliding window. Given a pixel X_{ij}, the corresponding output using CWM filters can be defined as

$$Y_{ij} = \text{median}\{X_{i-s,\,j-t},\ w_c \diamondsuit X_{ij} | (s,\,t) \in W,\ (s,\,t) \neq (0,\,0)\} \tag{2}$$

where w_c is the center weight and operator $\diamondsuit$ denotes repetition operation. In other words, $w_c \diamondsuit X_{ij}$ means that there are w_c copies of X_{ij} in total. Square window W is defined in terms of the image coordinates surrounding the origin X_{ij}. For instance, a 3×3 window is given by $W = \{(s,\,t) | -1 \leq s \leq 1,\ -1 \leq t \leq 1\}$, and the median is computed based on those $8 + w_c$ pixel values.

Note that integer w_c is positive and odd, and the CWM filter degenerates into standard median (SM) filter when $w_c = 1$. On the other hand, when w_c is equal to or larger than the sliding window size (e.g., $w_c \geq 9$ for a 3×3 window), the CWM filter becomes an *identity filter*, which always takes the origin pixel value X_{ij} as the output. Based on these observations, the performance of CWM filter with a larger center weight is superior to the one with a smaller center weight in detail preservation, but inferior in noise reduction [3]. Therefore, there exists a tradeoff between detail preservation and noise suppression in any median filter.

In order to effectively remove impulse noise as described in (1) while preserving image details, ideally the filtering should be applied only to the corrupted pixels, and the noise-free pixels should be kept unchanged. This can be achieved by determining whether the current pixel is corrupted, prior to possibly replacing it with a new value. Decision-based filters correspond to a well-known class of filters that appear to be particularly efficient to reduced impulse noise [2]. In this work, we propose an impulse detection scheme by successfully combining the SM filter with CWM filter. The construction of tri-state decision framework is described in Section II. The experimental results on a set of commonly used images are presented in Section III. Finally, the correspondence is concluded in Section IV.

II. Proposed Scheme

A novel and effective median filter, called *tri-state median* (TSM) filter, is proposed and discussed in this section. Noise detection is realized by an impulse detector, which takes the outputs from the SM and CWM filters and compares them with the origin or center pixel value in order to make a tri-state decision. The switching logic as shown in Fig. 1 is controlled by a threshold T ($\in [0,\,255]$ for gray-scale images), and the output of TSM filter is obtained by

$$Y_{ij}^{\text{TSM}} = \begin{cases} X_{ij} & T \geq d_1; \\ Y_{ij}^{\text{CWM}} & d_2 \leq T < d_1; \\ Y_{ij}^{\text{SM}} & T < d_2 \end{cases} \tag{3}$$

where Y_{ij}^{CWM} and Y_{ij}^{SM} are the outputs of CWM and SM filters, respectively, and $d_1 = |X_{ij} - Y_{ij}^{\text{SM}}|$ and $d_2 = |X_{ij} - Y_{ij}^{\text{CWM}}|$. Mathematically, it can be shown that $d_2 \leq d_1$ as follows.

Let $\{X_1,\,X_2,\,\cdots,\,X_z\}$ be the pixel intensity values sorted in ascending order, that is, $X_i \leq X_{i+1}$ $(i = 1,\,\cdots,\,z-1)$, where z denotes the window size and X_c be the origin pixel value. Therefore, $Y^{\text{SM}} = X_{(z+1)/2}$ and $d_1 = |X_c - X_{(z+1)/2}|$. Consider that the CWM filter has a center weight w_c and $1 \leq w_c \leq z$ to be meaningful, there are $z + w_c - 1$ values in total since $w_c - 1$ copies of the origin pixel value (i.e., X_{ij}) are inserted into the original sequence. Based on the sorted sequence $\{X_1,\,X_2,\,\cdots,\,X_z\}$, three nonoverlapping ranges require to be considered separately as follows (refer to Fig. 2 for the case of $z = 9$ and $w_c = 3$).

Suppose that the origin value X_c is located as the cth value in $\{X_1,\,X_2,\,\cdots,\,X_z\}$. First, in case that $(z+1)/2 - (w_c - 1)/2 \leq c \leq (z+1)/2 + (w_c - 1)/2$ [i.e., $(z - w_c + 2)/2 \leq c \leq (z + w_c)/2$, denoted as Region II in Fig. 2], we obtain that $Y^{\text{CWM}} = X_c$ and hence, $d_2 = 0 \leq d_1$. Second, if $c > (z + w_c)/2$ (i.e., Region III in Fig. 2), it can be deduced that $Y^{\text{CWM}} = X_{(z+w_c)/2}$ and we get

$$\begin{aligned} d_2 &= \left|X_c - X_{(z+w_c)/2}\right| = X_c - X_{(z+w_c)/2} \\ &\leq X_c - X_{(z+1)/2} = \left|X_c - X_{(z+1)/2}\right| = d_1. \end{aligned}$$

Third, when $c < (z - w_c + 2)/2$ (i.e., Region I in Fig. 2), it can be inferred that $Y^{\text{CWM}} = X_{(z-w_c+2)/2}$ and hence

$$\begin{aligned} d_2 &= \left|X_c - X_{(z-w_c+2)/2}\right| = X_{(z-w_c+2)/2} - X_c \\ &\leq X_{(z+1)/2} - X_c = \left|X_c - X_{(z+1)/2}\right| = d_1. \end{aligned}$$

Therefore, the definition of (3) follows the property that $d_2 \leq d_1$.

The capabilities of preserving image details inherited by the identity filter, the CWM filter and the SM filter descend in the above-mentioned order. On the aspect of noise suppression, in contrast, they ascend in the same order. An attractive merit of the proposed TSM filtering scheme is that it provides an adaptive decision to detect local noise simply based on the outputs of these filters. As a result, impulse noise can be removed for those corrupted pixels through SM or CWM filtering. For those uncorrupted pixels identified, they remain unchanged in order to preserve the local image details. Consequently, the tradeoff between suppressing noise and preserving detail is well balanced.

Note that the threshold T affects the performance of impulse detection. In the following section, we study T's influence on the

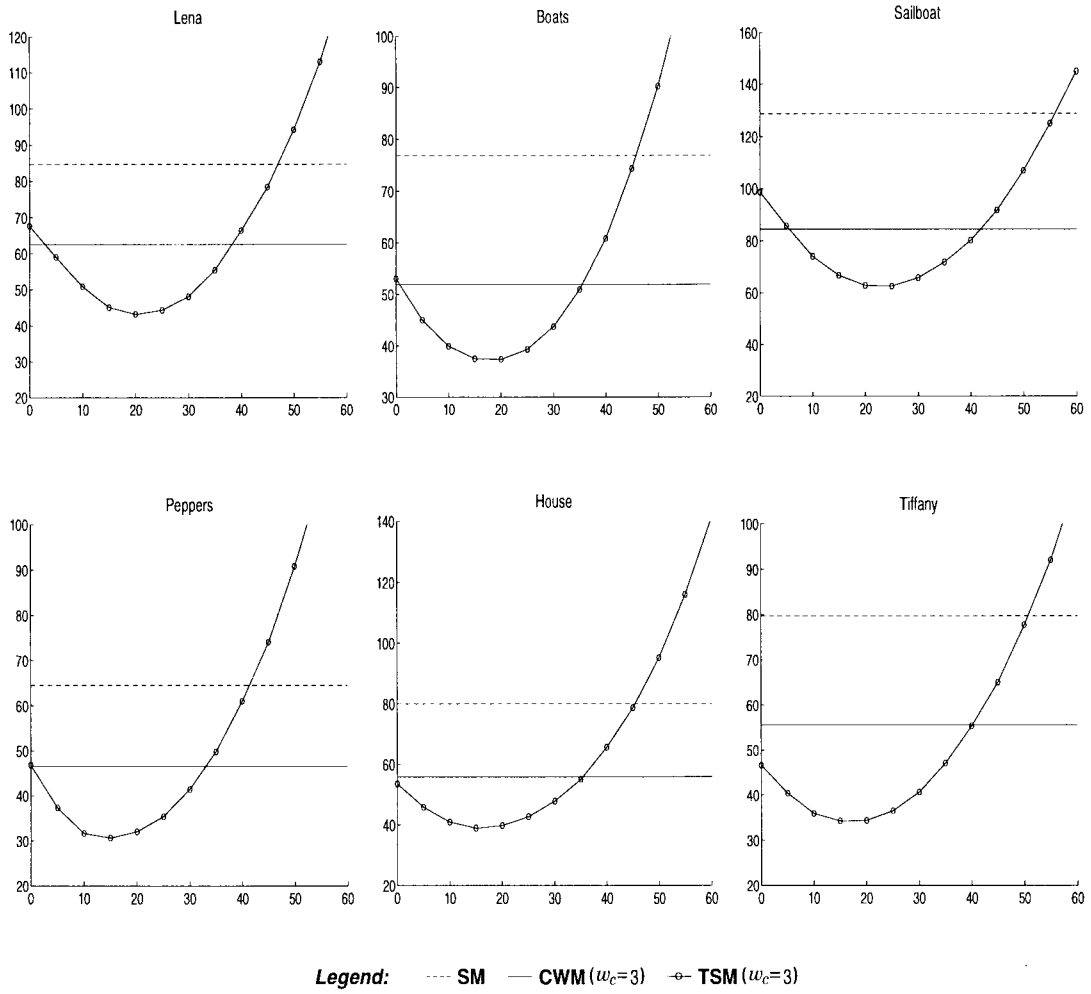

Fig. 3. Resulted MSE values (Y-axis) versus different thresholds T (X-axis) for multiple test images.

filtering performance through extensive computer simulation using a variety of test images.

III. Simulation Results

To quantitatively measure the performance of proposed TSM filtering scheme versus other median filters, the *mean square error* (MSE) criterion is utilized as follows:

$$\text{MSE} = \frac{1}{MN} \sum_{i=1}^{M} \sum_{j=1}^{N} (S_{ij} - Y_{ij})^2 \tag{4}$$

where M and N are the height and width of the image, respectively. Quantities S_{ij} and Y_{ij} denote the pixel values of uncorrupted and filtered images, respectively.

Commonly exploited test images have been experimented, and each image has 20% (i.e., $p = 0.2$) of total pixels being corrupted by impulse noise which is uniformly distributed over the range of $[0, 255]$. For performance comparison, all the median filters apply a 3×3 window, which slides from pixel to pixel in raster scanning order. CWM and TSM filters are tested on various images for the two values of center weight, i.e., $w_c = 3$ and $w_c = 5$. Simulation results clearly indicate that the performance in the case of $w_c = 3$ is superior.

The MSE values obtained by varying the threshold T for different test images are graphically presented in Fig. 3. It can be seen that the MSE performance is significantly improved by using our TSM filter with appropriate thresholds. Note that small MSE values usually occur when the threshold T employed by a TSM filter lies approximately in the range of $[10, 30]$ for $p = 0.2$. It is interesting to further observe that this threshold range is quite consistent and common to a wide variety of test images as shown in Fig. 3; thus, its performance is fairly stable.

With proper selection of threshold T, the TSM filtering scheme consistently offers improved visual quality of filtered images in addition to much reduced MSE values. Referring to Fig. 4, one can easily see that the noise suppression and detail preservation are satisfactorily compromised by using our TSM filter (e) as compared to using the other two median filters (c) and (d), respectively.

For different values of noise density p, optimum threshold range for yielding smallest MSE values and good visual quality can be obtained through similar simulation experiments.

IV. Conclusions

In this work, a new median filter, called tri-state median (TSM) filter, is introduced. By incorporating the SM filter and the CWM filter [3] into an impulse noise detection framework, a tri-state switching or decision mechanism is formed for effectively reducing impulse noise while preserving image details. Given a specified threshold T, the output of our proposed TSM filter may correspond

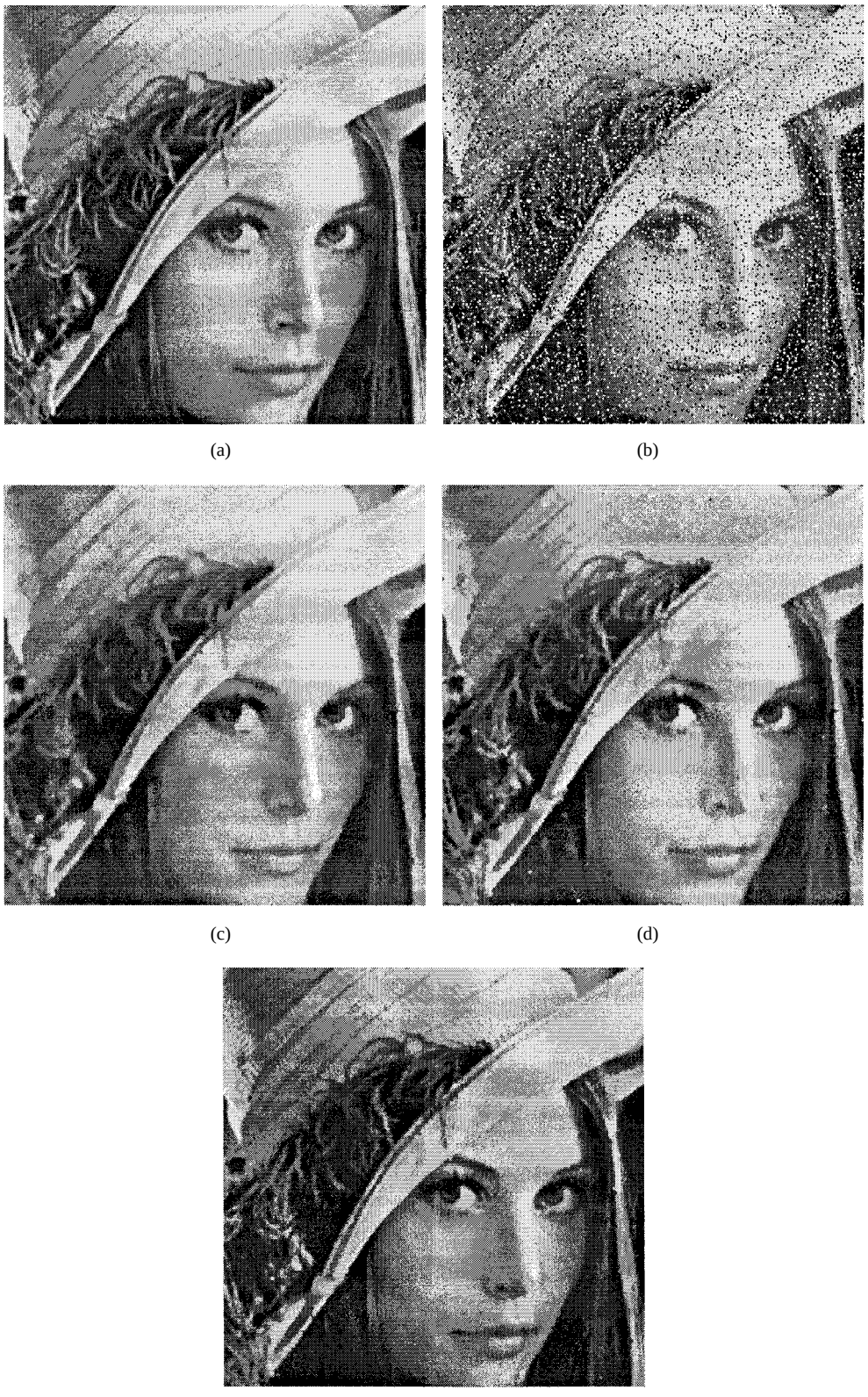

(a) (b) (c) (d) (e)

Fig. 4. (a) Original Lena image; (b) noisy image with $p = 0.2$, MSE $= 1472.16$; (c) SM filtered image, MSE $= 84.67$; (d) CWM filtered image, $w_c = 3$, MSE $= 62.57$; and (e) TSM filtered image, $T = 20$, $w_c = 3$, MSE $= 43.20$.

to one of three possible states, namely the origin pixel value (i.e., the pixel is noise-free), the SM filtered output (i.e., the pixel is corrupted), or the CWM filtered output (i.e., the pixel is probably uncorrupted with $w_c > 1$). Our proposed filtering framework has a simple computational structure and greatly outperforms the SM and CWM filters on the aspects of both MSE values and perceptual image quality. In addition, the proposed filter presents a quite stable performance over a wide variety of images, provided that the

threshold is chosen in the range of $[10, 30]$ approximately for the case that noise density $p = 0.2$. The proposed methodology remains applicable to adjust the weight w_c and the threshold T according to different values of p through simulation. Therefore, it is fairly attractive for practical usage.

ACKNOWLEDGMENT

The authors wish to thank the anonymous referees for their comments that improved the presentation of this work.

REFERENCES

[1] I. Pitas and A. N. Venetsanopoulos, *Nonlinear Digital Filters: Principles and Applications.* Boston, MA: Kluwer, 1990.

[2] J. Astola and P. Kuosmanen, *Fundamentals of Nonlinear Digital Filtering.* Boca Raton, FL: CRC, 1997.

[3] S.-J. Ko and Y.-H. Lee, "Center weighted median filters and their applications to image enhancement," *IEEE Trans. Circuits Syst.*, vol. 38, pp. 984–993, 1991.

Real-Time Restoration of Images Degraded by Uniform Motion Blur in Foveal Active Vision Systems

Giorgio Bonmassar and Eric L. Schwartz

***Abstract*— Foveated, log-polar, or space-variant image architectures provide a high resolution and wide field workspace, while providing a small pixel computation load. These characteristics are ideal for mobile robotic and active vision applications, but have been little used due to the general lack of image processing tools that are applicable to the log-polar coordinate system. Recently, we have described a generalization of the Fourier transform (the fast exponential chirp transform), which allows frame-rate computation of full-field two-dimensional (2-D) frequency transforms directly in log-polar coordinates. In the present work, we show that is possible to achieve full-frame image de-blur at frame rate on a standard "PC" platform, using these methods. We illustrate this idea with a Wiener filter based restoration technique. The main contribution of this note is the implementation of (space-variant) image de-blur directly in log-polar coordinates, using the exponential chirp transform. The results show reasonable quality of de-blur, and suggest that these methods are relevant to applications in mobile image processing platforms in which real-time motion deblur is important, and for which it is not desirable to use extensive or custom fabricated hardware.**

I. INTRODUCTION

Active vision systems, particularly in mobile applications, must contend with image blur caused by camera and object motion. This provides a natural application area for image restoration and deblur. However, image restoration is a computationally intensive process which is problematic in real-time systems. Much of the existing research in this area (see [1] for review) is oriented toward "off-line" computation, although several VLSI chips have been introduced for motion compensation [2], [3].

In the present work, it is demonstrated that a simple and well known approach to image restoration, based on Wiener filtering, can be implemented and executed at real-time rates, using a newly developed algorithm, the exponential chirp transform (ECT) [4]. We emphasize that this paper describes an application of a well-known deblur technique, which has been implemented in log-polar coordinates, rather than an investigation into image restoration *per se*. The main significance of this work is the demonstration, for the first time, that it is possible to provide full-frame image deblur, operating directly in log-polar coordinates, at real-time (i.e., 30 frames/s) rates.

The advantages of using log-polar coordinates have been summarized in [5]. This image format is favorable for active-vision tasks such as object tracking [6]–[8]. Briefly, it provides a form of lossy compression, trading off a wide-field of view and high-resolution sampling. In [5], it is shown that reductions in space-complexity (i.e., the number of pixels which must be processed per frame) in the range of two to four orders of magnitude can obtained via the use of log-polar coordinates. In this work, it is also mentioned that virtually all higher biological systems use some variant of this image architecture, presumably for the reason of reducing the space-complexity of image processing. The "retina" of monkeys and humans, with its well known "foveal" structure, is transformed via log-polar coordinates, into one of the brains internal representations of the visual field (see [9] for review). In image processing terms, the retinal representation of the visual field corresponds to a "pyramid" representation [10].[1] Because the pyramid representation involves no nonlinear coordinate transform (only a scale-change and resampling), conventional image processing may be applied, although there is an implementation problem involved at the discrete transitions between pyramid levels in "foveal" pyramid architectures. Log-polar representation does involve a nonlinear coordinate transform, summarized below, but provides a continuous multiscale representation of the visual field. The vast majority of work in multi-scale representation to date has been based on the pyramid data form, in part due to the lack of image processing tools that are applicable directly in log-polar coordinates. This situation has changed recently with the introduction of frequency domain techniques which are directly applicable in log-polar coordinates (i.e., the exponential chirp transform). This paper demonstrates the first application of this work to the problem of image restoration. We also point out that iterative use of Wiener filtering, as in the direct regularized restoration method (see [1] for review), is computationally similar, and so can be performed with the FECT-based method described here. In this work however, we show only a single step of iterative restoration, which in our real-time application domain, is a desirable compromise.

II. PREVIOUS WORK: LOG-POLAR COORDINATES AND THE EXPONENTIAL CHIRP TRANSFORM

The log-polar map illustrated in Fig. 1, is of interest in computer vision for two major reasons.

Manuscript received February 26, 1998; revised march 17, 1999. This work was supported by the National Science Foundation under Grant ITS 9812143. The associate editor coordinating the review of this manuscript and approving it for publication was Prof. Kannan Ramchandran.

G. Bonmassar is with the Harvard MGH-NMR Centrer, Charlestown, MA 02129 USA (e-mail: giorgio@nmr.mgh.harvard.edu).

E. L. Schwartz is with the Department of Cognitive and Neural Systems, Boston University, Boston, MA 02146 USA (e-mail: eric@thing4.bu.edu).

Publisher Item Identifier S 1057-7149(99)09346-X.

[1] The original work of [10] described a "full" pyramid, in which the size of the pyramid layers were all the same. More recently, "truncated" or "foveating" pyramids have been introduced in which there are increasingly smaller areas of the visual field devoted to the higher resolution layers of the pyramid [11]. It is the latter, rather than the former type of pyramid, which is "foveal" and which is of direct relevance to the present paper.